Available online at www.sciencedirect.com
SCIENCE DIRECT®
Acta Materialia 53 (2005) 3459–3468
Acta MATERIALIA
www.actamat-journals.com

Experiment and multiscale modeling of the coupled influence of constituents and precipitates on the ductile fracture of heat-treatable aluminum alloys

Gang Liu [a,b,*], Jun Sun [a,*], Ce-Wen Nan [b], Kang-Hua Chen [c]

[a] *State Key Laboratory for Mechanical Behavior of Materials, School of Material Science & Engineering, Xi'an Jiaotong University, Xi'an 710049, China*

[b] *State Key Laboratory of New Ceramics and Fine Processing, and Department of Materials Science and Engineering, Tsinghua University, Beijing 100084, China*

[c] *State Key Laboratory for Powder Metallurgy, The University of Southern Central China, Changsha 410083, China*

Received 5 October 2004; received in revised form 31 March 2005; accepted 4 April 2005
Available online 10 May 2005

Abstract

Solution and quench treatments are very important for the heat-treatable aluminum alloys because any change in these treatments will induce a trade-off in volume fraction between the constituents and precipitates and so will cause a change in the mechanical properties. In this paper, three types of solution + quench treatments were applied to two kinds of aluminum alloys, i.e., the Al–Cu–Mg alloy that contains disc/plate-shaped precipitates and the Al–Mg–Si alloy that contains rod/needle-shaped precipitates, to change the relative content between the constituents and the precipitates and to develop different coupling of the constituent and precipitates. The specimen treated with an enhanced solution or a stepped solution is found to exhibit a significant increase in yield strength, ductility, and fracture toughness. A multiscale model is presented to quantitatively estimate the coupled influence of the constituents and precipitates on the mechanical properties by combining with a strengthening model. The experimentally observed non-monotonic dependence of ductility on the trade-off in volume fraction between the constituents and precipitates is reasonably explained by using this multiscale model. In addition, the influence of stress triaxiality level on the ductility and fracture toughness is also calculated. All the calculations are in quite good agreement with the experimental results.

Keywords: Aluminum alloys; Toughness; Ductility; Precipitation; Modeling

1. Introduction

Low density combined with high strength have made heat-treatable aluminum alloys the primary materials of choice for applications such as in aircraft, where the specific strength (strength-to-weight ratio) is a major design consideration. However, the low fracture toughness limits the extensive application of commercial heat-treatable aluminum alloys. The coarse second phase particles, termed constituents in aluminum alloys, are mainly responsible for the low fracture resistance because the constituents are usually the void/crack initiators or the preferential crack paths [1]. Therefore, lowering the volume fraction of constituents has been regarded as the most important approach to improve the fracture toughness for the aged aluminum alloys [2–4].

The formation of constituents in aged aluminum alloys primarily results from the presence of impurities,

* Corresponding authors. Tel.: +86 29 82667143; fax: +86 29 82663453 (J. Sun).
E-mail addresses: lgsammer@mailst.xjtu.edu.cn, lgsammer@mail.tsinghua.edu.cn (G. Liu), junsun@mail.xjtu.edu.cn (J. Sun).

1359-6454/$30.00
doi:10.1016/j.actamat.2005.04.002

e.g., Fe and Si, and excessive amounts of major alloying elements such as Mg, Zn, and Cu. This means that the decrease of the iron and silicon levels and hence the volume fraction of constituents would improve the fracture toughness [5,6]; this approach has been employed in the development of 2124, 7050, 7175, and 7475 aluminum alloys. However, the improvement of fracture toughness by purification is limited because the complete removal of impurities is hard to achieve especially in commercial aluminum alloys. Besides the constituents resulting from the presence of impurities and excessive alloying elements, another kind of constituent is present in the commercial aluminum alloys, which contains alloying elements as well but results from the non-equilibrium solidification due to the lower solvus limit of the alloying elements in aluminum. In principle, this kind of constituent is soluble and could be dissolved into the solid solution reversibly through solution treatment. It is then possible to develop another effective approach to improving the fracture toughness by solubilizing these soluble constituents by applying an enhanced solution treatment.

The enhanced solution treatment is a stepped solution treatment, in which the solution treatment will be performed at temperatures which is gradually elevated with time. In comparison, the traditional solution treatment is usually performed at a stationary temperature and, in order to avoid the presence of transient liquid phase, the stationary temperature will be greatly limited so as not to exceed the melting point of multiphase eutectic. Since each of eutectic phases dissolves into the matrix in a certain sequence during solution treatment, the eutectic temperature will be elevated with the complete solution of one of the eutectic phases. This indicates that the upper temperature limit for solution will gradually increase during the treatment and so the application of traditional solution treatment with a stationary lower temperature could not dissolve as much soluble constituents as possible. In contrast, the application of stepped solution treatment with a gradual increase in temperature could both avoid exceeding the eutectic melting and realize the complete solution of dissolvable constituents. So the enhanced solution treatment or stepped solution treatment has a potential for industrial application. However, little work has been carried out on the application of stepped solution treatment and some limited results showed that the aged aluminum alloys treated by the stepped solution treatment exhibited greater strength [7,8]. But most importantly, the enhanced solution treatment should have a significant influence on the ductile fracture of aluminum alloys, which has not been studied up to now.

The application of enhanced solution treatment is believed to decrease the volume fraction of constituents. At the same time, the solution of dissoluble constituents will make more alloying elements dissolve into the matrix and so will induce more strengthening second phase particles to be precipitated. This indicates that a trade-off in volume fraction between the constituents and precipitates will be achieved by applying the enhanced solution treatment. Because the independent decrease of coarse constituents should be favorable for enhancing the fracture resistance while the independent increase of strengthening precipitates should induce somewhat contrary results, the trade-off in volume fraction between the constituents and the precipitates will be possible to create a non-monotonic evolution trend of the ductility or of the fracture toughness. For analysis purposes, there is an urgent need to understand the combined influence of both the constituents and the precipitates on the ductile fracture. It has been well known that the coarse constituents in aluminum alloys are from several to tens of micrometers in diameter, depending on the fabrication procedure, and the fine strengthening precipitates are tens of nanometers in size, hundreds of times less than that of constituents [9]. In addition, there exists another kind of second phase particle of intermediate size between the constituents and precipitates, termed dispersoids, in the commercial aluminum alloys (see Fig. 1) and all three kinds of the second phase particles contribute to the fracture behaviors simultaneously. Therefore, the combined influence of both the constituents and the precipitates is essentially a multiscale coupling that should connect the microstructural features from micrometer-scale length to nanometer-scale length [10–13]. There have been rare studies on the multiscale coupling of second phase particles intrinsically contained in aged aluminum alloys, so the application of enhanced solution treatment should motivate not only some technological attention but also some theoretical attention especially on the modeling and simulation of the combined influence of multiscale-sized second phase particles on the ductile fracture.

In this paper, we focus on the experimental and theoretical investigations of the combined influence of coarse constituents and fine precipitates on the ductile fracture in heat-treatable aluminum alloys. Three types of solution + quench treatments, including an enhanced solution treatment, have been applied to two typical heat-treatable aluminum alloys, i.e., Al–Cu–Mg alloy containing disc- or plate-shaped strengthening precipitates and Al–Mg–Si alloy containing rod- or needle-shaped strengthening precipitates, respectively, to study the coupled influence of constituents and precipitates on the ductile fracture and to study the improvement of ductility and fracture toughness by applying the enhanced solution treatment. The changes in volume fractions of second phase particles as well as the changes in quasi-stationary mechanical properties were experimentally measured for comparison. With consideration of the significant influence of stress triaxiality level on the constituent cracking or decohesion, the dependence of

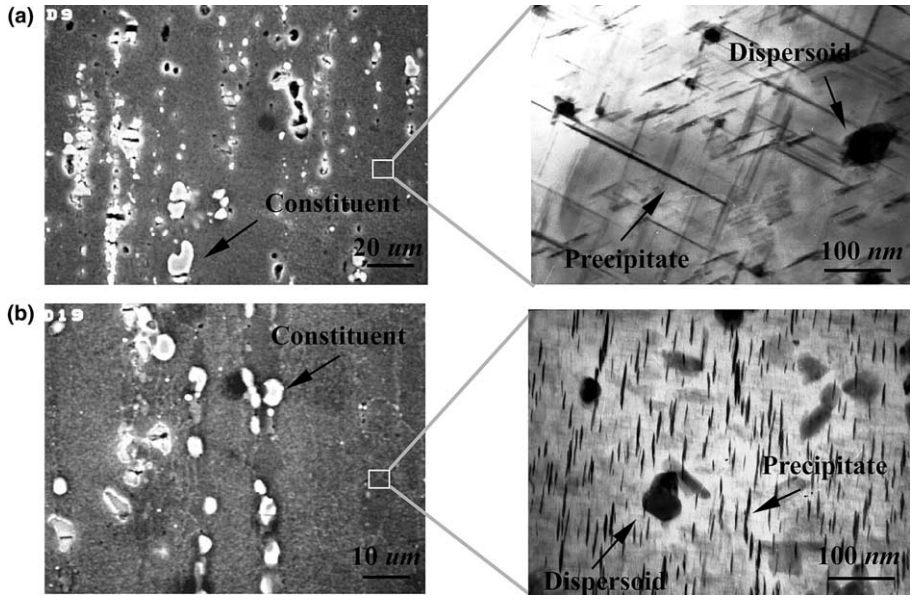

Fig. 1. SEM and TEM images illustrating the three kinds of second phase particles with different sizes and morphologies in the (a) Al–Cu–Mg alloy and (b) Al–Mg–Si alloy.

strain to fracture or tensile ductility on the stress triaxiality level was investigated as well. A multiscale fracture model [14,15] was presented to estimate the coupled influence of second phase particles on the ductility and fracture toughness of aged aluminum alloys and the calculations were found to fit well with the experimental results.

2. Experimental procedures

2.1. Materials and processing

The aluminum alloys used in present experiment were hot-rolled Al–Cu–Mg plate of 16 mm thickness and extruded Al–Cu–Mg and Al–Mg–Si rods of 18 mm diameter, both supplied by the research laboratory of Xi'an Aircraft Industry Ltd. The Al–Cu–Mg plate and the Al–Cu–Mg rod were from the same ingot. The composition in weight percentage is 4.62% Cu, 0.65% Mg, 0.22% Mn, 0.08% Si, 0.1% Fe, 0.1% Zn, and balance Al for Al–Cu–Mg alloy and 1.12% Mg, 0.57% Si, 0.25% Cu, 0.22% Cr, and balance Al for Al–Mg–Si alloy.

Three types of solution + quench treatment were applied on the two aluminum alloys for comparison, i.e., enhanced solution + fast quench treatment (abbreviated as EF), traditional solution + fast quench treatment (TF), and traditional solution + slow quench treatment (TS). The traditional solutions for the Al–Cu–Mg and Al–Mg–Si alloys were treated at 766 K for 2 h and at 703 K for half-an-hour, respectively. The fast quench treatment refers to quenching into cold water while the slow quench treatment means cooling with a controlled rate of 5 K/s. The enhanced solution for Al–Cu–Mg alloy involved first treating at 766 K for 2 h, followed by an increase in treatment temperature up to 776 K with a rate of 4 K/h; for the Al–Mg–Si alloy, the first treatment was at 703 K for half-an-hour, followed by an increase in treatment temperature up to 708 K with a rate of 7 K/h. The maximum error of all the temperature measurements was ±1 K.

The Al–Cu–Mg alloy and Al–Mg–Si alloy were artificially aged at 513 K and at 463 K for various times from 0.25 h to 10 days to get different aging conditions.

2.2. Microstructural determination

The microstructures of sectioned Al–Cu–Mg and Al–Mg–Si rods were examined using optical microscopy. Metallographic preparation involved methods of standard surface preparation. The specimens were etched with Keller's etchant. Based on quantitative microscopy [16], the size and volume fraction of the three populations of second phase particles in the aluminum alloys, i.e., coarse micrometer-sized ellipse-shaped constituents, intermediate sub-micrometer-sized sphere-shaped dispersoids, and fine nanometer-sized plate/disc-shaped (in Al–Cu–Mg alloy) or rod/needle-shaped (in Al–Mg–Si alloy) precipitates, were quantitatively measured by using scanning electron microscope (SEM) and transmission electron microscope [14,15,17]. For example, the volume fraction of the coarse constituent was measured at a magnification of 400 times by using point counting with a grid containing 900 points. Six random views of each of three specimens per alloy were examined. The distribution of the constituents within each

alloy was regarded as random; therefore, the volume fraction, V_c, is given by P_p which is the fraction of total grid points that fall on constituent particles. Constituents smaller than 0.1 μm were ignored. Using a Hitachi S-2700 SEM, the size measurements of the constituents were performed on sectioned profiles of the untested specimens. Since the constituents were irregular in shape, an effective particle diameter, d_c, was defined as $d_c = \sqrt{d_1 d_2}$, where d_1 and d_2 are the smallest and largest dimensions of a coarse constituent, respectively. The mean radius, $\bar{r}_c$, of n particles is then given by $\bar{r}_c = (\sum_{i=1}^{n} \sqrt{d_1 d_2})/2n$. In order to obtain the accurate size of the particles, at least 150 random particles were measured for all three kinds of particles.

2.3. Mechanical measurement

The fracture toughness of Al–Cu–Mg alloys was characterized with compact tension (CT) specimens and the R curve method. Both the L–T and T–L orientation (refer to Fig. 2) specimens were measured and all the specimens had a size of 62.5 mm width and 6.25 mm thickness. Prior to the fracture toughness experiment, the specimens were fatigue cracked at a constant stress ratio ($R = K_{min}/K_{max}$) of 0.1 and under decreasing stress intensity condition. Strictly conforming to ASME 561, the fracture toughness experiments were performed on a servohydraulic Instron-type testing machine by using potential-drop methodology to measure crack length. The measured data were analyzed to determine the plane strain fracture toughness at crack initiation [18].

Dog-bone-shaped tensile specimens with a gauge size of 6 mm diameter and 40 mm length were used to measure the yield strength, the strain to fracture, and the strain hardening exponent, and notched tensile specimens with a circumferential notch at the center part were used to determine the dependence of strain to fracture on stress triaxiality level. All the specimens have an axis along the longitudinal direction. The tensile test was performed at a constant strain rate of $5 \times 10^{-4}\ s^{-1}$ with the load direction parallel to the specimen axis. The yield stress was determined as the 0.2% offset and the strain to fracture was determined as $\varepsilon_f = \ln(A_0/A_f)$, where A_0 is the initial area and A_f is the area at fracture of the specimens. Six different notch radii (r) were used in the notched specimens in order to vary stress states. The stress states in such specimens can be characterized by $\sigma_m/\bar{\sigma}$, the ratio of mean σ_m to equivalent stress $\bar{\sigma}$ following conventional definitions [19], and is given approximately by $\sigma_m/\bar{\sigma} = 1/3 + \ln(a/2r + 1)$ [20,21], where a is the radius of the notch ligament. The values of r were chosen here to achieve different stress triaxiality levels of $\sigma_m/\bar{\sigma}$ ranging from 0.54 to 1.06.

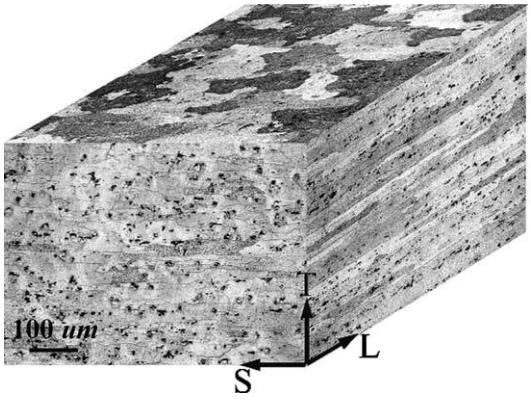

Fig. 2. Triplanar optical micrograph of the Al–Cu–Mg plate and the definition of orientations.

3. Experimental results

3.1. Microstructures

Figs. 3 and 4 show the optical micrographs of sectioned Al–Cu–Mg and Al–Mg–Si rods, respectively, with different treatments. It is found that the change in grain size with different treatment is not noticeable, as shown at Table 1 where L and w are the averaged grain length and grain width, respectively, and the values in parentheses are the corresponding standard deviations. However, the EF-treated specimens (Figs. 3(c) and 4(c)) contain fewer constituents while the TS-treated specimens (Figs. 3(a) and 4(a)) contain more constituents compared with the TF-treated specimens (Figs. 3(b) and 4(b)). Besides, less aggregation or contact of the constituents is observed in an optical view and very small constituents are absent in the EF-treated specimens. These indicate that the application of the enhanced solution treatment facilitates the dissolution of the soluble constituents and hence the decrease in the volume fraction of constituents. On the other hand, the volume fraction of precipitates at peak-aged condition increases, as listed in Table 1 where the volume fraction and size of the three kinds of second phase particles are summarized as well. On the contrary, the application of TS treatment causes an increase in the content of constituents and a decrease in the content of precipitates. It is then concluded that a trade-off in volume fraction between the constituents and precipitates has been achieved by applying the three types of treatment. Some interesting results can be found in Table 1, which show that the constituents in EF-treated specimens have a larger size than that of constituents in TF-treated specimens. This is because more small constituents have been dissolved after EF treatment and so the surviving large constituents should have a larger average size (the size is determined with an averaging method of quantitative microscopy). However, the

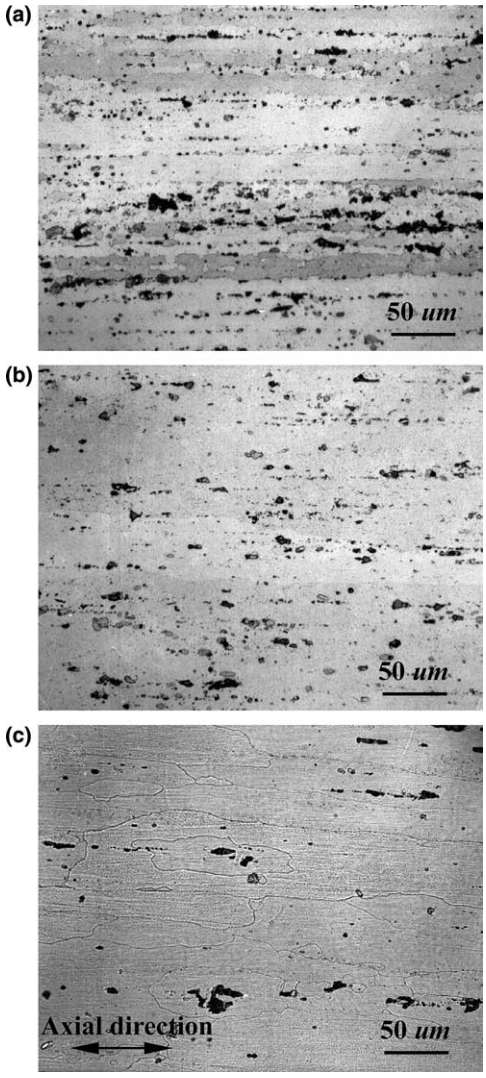

Fig. 3. Typical micrographs of the sectioned Al–Cu–Mg rod treated with (a) TS, (b) TF, and (c) EF.

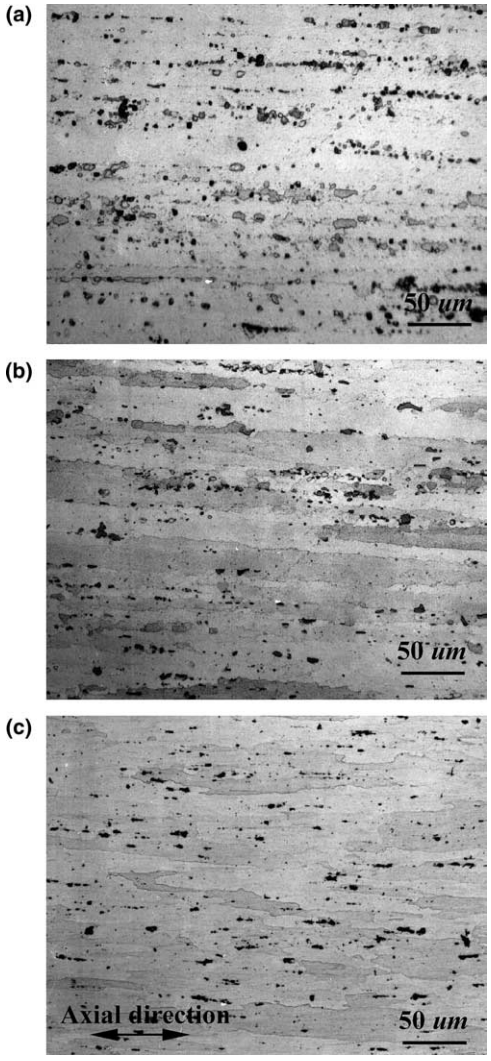

Fig. 4. Typical micrographs of the sectioned Al–Mg–Si rod treated with (a) TS, (b) TF, and (c) EF.

standard deviations of the particle parameters are smaller for the EF-treated specimens.

3.2. Smooth specimens and CT specimens

The variation of yield strength of Al–Cu–Mg alloy and Al–Mg–Si alloy with aging time was experimentally measured from the smooth tensile specimens, as depicted in Fig. 5(a) and (b), respectively. Owing to the dissolution of more alloying atoms into the matrix caused by the enhanced solution treatment, the EF-treated specimens exhibit greater peak-aged yield strength (increase by about 20% for both the two alloys) than the TF-treated specimens. On the contrary, the TS-treated specimens have lower peak-aged yield strength (decreased by about 13% for Al–Cu–Mg alloy and about 16% for Al–Mg–Si alloy) than the TF-treated specimens because the slow quench treatment makes many alloying atoms precipitate from the saturated solid solution to form constituents. The curves in Fig. 5 are calculated by using a recent strengthening model [17] together with some calibrated parameters from present experiments. The calculated curves are in good agreement with the measured values and it is necessary to note that, although many similar models have been established to describe the variation of yield strength with aging time for heat-treatable aluminum alloys [22–26], the model presented by the authors was specifically applicable for the heat-treatable aluminum alloys containing either disc/plate-shaped precipitates or rod/needle-shaped precipitates.

The strain to fracture (ε_f) and fracture toughness (K_{IC}) of the aluminum alloys were measured from the smooth tensile specimens and from the CT specimens, respectively, and the values at peak-aged condition are summarized in Table 2. The EF-treated specimens

Table 1
Parameters of the three kinds of second phase particles and grain size

Alloy/ treatment	Constituents			Dispersoids			Precipitates[a]			Grain size	
	f_c (vol.%)	r_c (μm)	L_l/L_s[b]	f_d (vol.%)	r_d (μm)	k_d	f_p (vol.%)	r_p (nm)	k_p	L (μm)	w (μm)
Al–Cu–Mg											
EF	2.55	4.32 (0.27)	3.4 (0.12)	0.15	0.04 (0.01)	1.05 (0.02)	6.27	105 (3.2)	22 (0.7)	1319 (47)	122 (26)[c]
TF	4.83	4.11 (0.83)	3.2 (0.44)	0.18	0.08 (0.03)	1.11 (0.02)	3.64	120 (5.6)	26 (1.7)	1245 (39)	117 (18)
TS	5.25	3.85 (1.35)	2.9 (0.81)	0.23	0.11 (0.05)	1.14 (0.04)	3.06	125 (9.1)	28 (3.8)	1221 (37)	110 (19)
Al–Mg–Si											
EF	2.35	2.53 (0.16)	2.2 (0.08)	0.09	0.02 (0.01)	1.06 (0.02)	2.74	32 (1.7)	31 (1.1)	773 (35)	58 (21)
TF	3.46	2.41 (0.58)	2.1 (0.36)	0.11	0.03 (0.02)	1.22 (0.03)	1.82	35 (4.4)	34 (2.3)	726 (31)	49 (14)
TS	4.14	2.23 (0.95)	1.9 (0.67)	0.12	0.06 (0.04)	1.35 (0.03)	1.41	37 (7.8)	36 (3.6)	711 (30)	48 (12)

[a] At peak-aged condition.
[b] L_l and L_s are the longer size and shorter size of the constituents, respectively. For L–T specimens, k_c is equal to L_l/L_s, while for T–L specimens, k_c is the reciprocal of L_l/L_s.
[c] The values in parentheses are standard deviations.

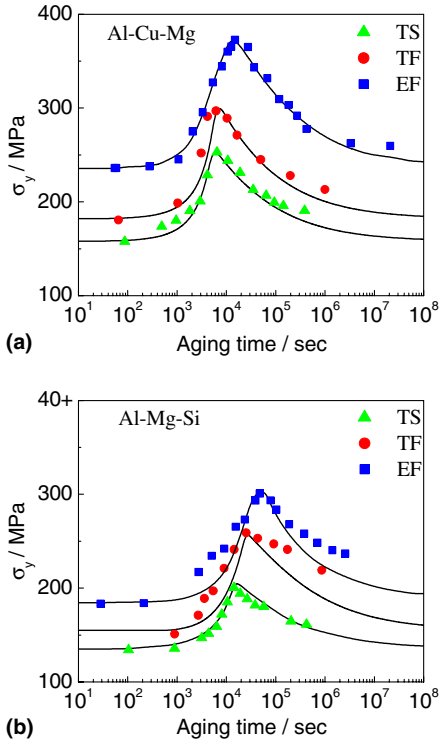

Fig. 5. Variation of yield strength (σ_y) with aging time for (a) Al–Cu–Mg alloy and (b) Al–Mg–Si alloy. The triangle dots (green), solid dots (red), and square dots (blue) are the experimental results of specimens treated with TS, TF, and EF, respectively. The curves are calculated by using the strengthening model [17]. (For interpretation of the references in colour in this figure legend, the reader is referred to the web version of this article.)

exhibit much larger enhancement in both ε_f and K_{IC} compared with the TF-treated specimens, which indicates that the enhanced solution treatment should have significant potential for industrial application. It is also found in present experiments that, although the change trend of both ε_f and K_{IC} with aging time is contrary to that of the yield strength as usually observed by others [27], the change trend of ε_f with different solution + quench treatments is unusual, i.e., the dependence of ε_f on treatments is non-monotonic. In other words, ε_f of both the EF-treated and the TS-treated specimens is larger than that of the TF-treated counterpart (see Table 2), although the EF-treated and the TS-treated specimens contain the least and the most constituents, respectively. This should be attributed to the coupled influence of both the constituents and precipitates on the ductility, which will be discussed later.

Table 2
Mechanical properties of the two alloys with different treatments

Alloy/treatment	σ_y (MPa)	ε_f	K_{IC} (MPa m$^{1/2}$)	
			L–T	T–L
Al–Cu–Mg				
EF	353	0.289	28.43	18.58
TF	298	0.237	22.68	14.26
TS	258	0.249	19.91	12.10
Al–Mg–Si				
EF	292	0.341	–	–
TF	259	0.275	–	–
TS	225	0.288	–	–

3.3. Notched specimens

The dependence of the strain to fracture of the two peak-aged alloys on the stress triaxiality level was measured from the notched tensile specimens and summarized in Table 3. The strain to fracture of the EF-treated specimens is found to be less sensitive to the stress conditions while that of the TS-treated specimens is significantly sensitive to the stress conditions. The difference in volume fraction of constituents should be responsible for such a difference in sensitivity.

Table 3
Strain to fracture of the two alloys under different constraint conditions

Alloy/treatment	$\sigma_m/\bar{\sigma}$					
	0.54	0.65	0.74	0.86	0.93	1.06
Al–Cu–Mg						
EF	0.266	0.229	0.200	0.186	0.178	0.176
TF	0.211	0.162	0.143	0.124	0.116	0.108
TS	0.218	0.150	0.137	0.118	0.100	0.087
Al–Mg–Si						
EF	0.332	0.295	0.272	0.259	0.246	0.228
TF	0.241	0.198	0.178	0.166	0.154	0.133
TS	0.246	0.187	0.172	0.153	0.130	0.108

4. Discussion

4.1. Coupled influence of both constituents and precipitates

Microstructural observations revealed that both the present two types of aluminum alloys, even after EF-treatment, fracture in a transgranular mode predominantly. So for simplicity, we neglect the influence of intergranular fracture. A multiscale model has been established by the authors [14,15] to describe the dependence of strain to fracture and fracture toughness on the three kinds of second phase particles intrinsically contained in commercial aged aluminum alloys. Some unified expressions have been also derived to relate ε_f and K_{IC} with the size and interparticle spacing of the three kinds of second phase particles as

$$\varepsilon_f = \frac{b\rho_g^c}{2\tilde{\varepsilon}_e(\theta)}\left[\frac{I}{0.405\pi h}\right]^{\frac{1}{n+1}}\left[\frac{\lambda_c}{2r_c}-1\right]^{\frac{1}{n+1}}(\lambda_d+\lambda_p)^{-1} \times\sqrt{[(1.7r_d\lambda_p)^2+(0.25\lambda_d\lambda_p)^2]}, \quad (1)$$

and

$$K_{IC} = \Gamma\sqrt{Bn^2\sigma_y\left[\frac{\lambda_c}{2r_c}-1\right]^{\frac{1}{n+1}}[(1.7r_d\lambda_p)^2+(0.25\lambda_p\lambda_d)^2]^{1/2}(\lambda_d+\lambda_p)^{-1}}, \quad (2)$$

with

$$\Gamma = \sqrt{\frac{CEb\rho_g^c}{2\tilde{\varepsilon}_e(\theta)}}, \quad (3)$$

and

$$B = [(1+3n)(5.39\sqrt{0.13+n}-2.53n)]^{\frac{1}{n+1}}, \quad (4)$$

where r_c is the size of ellipsoidal constituents perpendicular to external loading direction and r_d is the radius of sphere dispersoid; λ_i (i = c, d, and p) is the interparticle spacing of constituents, dispersoids, and precipitates, respectively; $\tilde{\varepsilon}_e(\theta)$ is an effective value of the proportionality constant $\tilde{\varepsilon}_{ij}(\theta)$, which is a dimensionless function of the angular variable θ in polar coordinates, and is a constant when $\theta = 0$; E and b are the elastic modulus and Burgers vector of matrix, respectively; C is a constant of ~1/40 and the critical dislocation density in the matrix, ρ_g^c can be regarded as a constant at room temperature; n is the strain hardening exponent and is experimentally measured as ~0.2 for Al–Cu–Mg alloys and ~0.3 for Al–Mg–Si alloys, respectively; I and h are functions of n [28,29]; σ_y is the yield strength and can be estimated by the age-strengthening model [17] that is based on the strengthening expressions for the aluminum alloys containing plate- or rod-shaped precipitates [30]. Some parameters such as ρ_g^c and $\tilde{\varepsilon}_e(0)$ are difficult to determine but they could be approximately regarded as constant, so the strain to fracture and fracture toughness calculated in this paper are normalized ones which are divided by some reference strain to fracture and fracture toughness, respectively, to eliminate these unknown parameters. The reference strain to fracture and the fracture toughness in the present paper are characterized by those given at special conditions such as $f_c = 0$ or $\sigma_m/\bar{\sigma} = 0.54$, which are independent of the heat treatment.

The size and interparticle spacing of the three kinds of second phase particles could be related to the volume fraction f as $f_i = c\pi k_i(r_i/\lambda_i)^3$ (i = c, d, and p) on an assumption of cubic arrangement, where k_i is the aspect ratio of the particles and the value of c is 2 for the non-spherical constituents and precipitates and 4/3 for the spherical dispersoids. Especially for the constituents, k_c is the ratio between the size parallel to the external loading direction and the size perpendicular to the loading direction. So Eqs. (1) and (2) both contain the terms of volume fraction of the three kinds of second phase particles as well, and the influence of trade-off in volume fraction between the constituents and the precipitates on both ε_f and K_{IC} could be calculated as shown in Figs. 6 and 7, respectively. It is found that the fracture toughness of the heat-treatable aluminum alloys is monotonically dependent on the trade-off in volume fraction between the constituents and the precipitates, e.g., the EF-treated specimens exhibit the largest fracture toughness while the TS-treated specimens exhibit the least fracture toughness (see Fig. 7). However, the dependence of ductility or strain to fracture on the trade-off in volume fraction between the constituents and the precipitates is somewhat complicated. As shown in Fig. 6, with the decrease in volume fraction of constituents and at the same time the increase of precipitates, the alloys that contain constituents of a large aspect ratio will exhibit a non-monotonic change on ε_f, i.e., ε_f initially decreases down to a minimum and then increases up to a much larger value at the vanishing of the constituents. This non-monotonic change is well verified by present experimental results of both the Al–Cu–Mg alloy and the Al–Mg–Si alloy. In contrast, the alloys that contain constituents of a

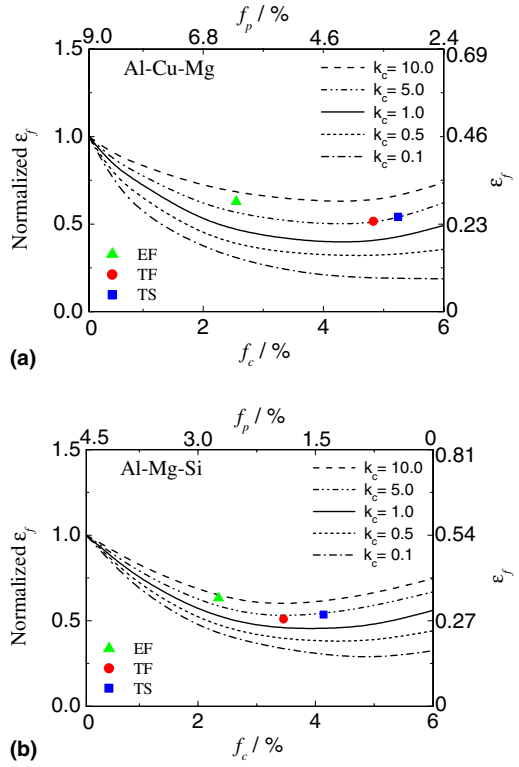

Fig. 6. Coupled influence of the constituents and precipitates on the strain to fracture (ε_f) for (a) Al–Cu–Mg alloy and (b) Al–Mg–Si alloy as a function of the aspect ratio of the constituents (k_c). The trade-off in volume fraction between the constituents and precipitates is considered. The square dots (blue), solid dots (red), and triangle dots (green) are the experimental results of specimens treated with TS, TF, and EF, respectively. The curves are calculated by using the present multiscale model. (For interpretation of the references in colour in this figure legend, the reader is referred to the web version of this article.)

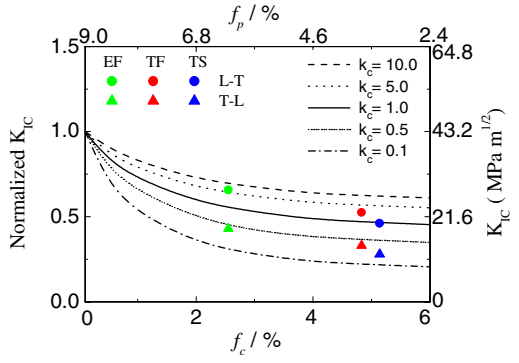

Fig. 7. Coupled influence of the constituents and precipitates on the fracture toughness (K_{IC}) for Al–Cu–Mg alloy as a function of the aspect ratio of the constituents (k_c). The trade-off in volume fraction between the constituents and precipitates is considered. The solid dots and triangle dots (green: EF, red: TF, blue: TS) are the experimental results of the L–T specimens and the T–L specimens, respectively. The curves are from calculations with present model. (For interpretation of the references in colour in this figure legend, the reader is referred to the web version of this article.)

low aspect ratio will exhibit a monotonic change of ε_f, similar to that of K_{IC}.

It is well known that the increasing of precipitates should have two main influences on the properties of aged aluminum alloys. One is to strengthen the matrix and the other is to induce more localization of stress or strain. The former influence is positive because it can enhance the fracture resistance but the latter is negative because it will reduce the ductility. On the other hand, the decrease of constituents will enhance both the fracture resistance and the ductility and the enhancement is significant especially when the constituents have a lower k_c. As a result, the trade-off in volume fraction between the constituents and the precipitates will cause a monotonic change for the ductility when the constituents have a lower aspect ratio. When the constituents have a larger aspect ratio, the change of ductility will be non-monotonic, as shown in Fig. 6. This indicates that the coupled influence of the constituents and the precipitates on ductility is dependent not only on the trade-off in volume fraction between the two kinds of second phase particles but also on the morphology of the particles especially of the constituents. However, the change of fracture toughness with different treatments is monotonic no matter what the aspect ratio of constituents is, which indicates that the decreasing of constituents is overwhelmingly effective in enhancing the fracture toughness.

Compared with the constituents of large aspect ratio (k_c), the constituents of small aspect ratio have a short interparticle spacing, which means that these constituents are easy to coalesce after breaking or debonding from the matrix. The coalescence of constituents will induce the formation of cracks and the accelerated propagation of a main crack. As a result, the specimens that contain constituents of small aspect ratio should exhibit a low fracture toughness and low ductility. This is partially responsible for the lower fracture toughness of T–L specimens than of L–T specimens (Fig. 7) because the constituents in the former have a small aspect ratio [14].

The agreement between the calculations and the experimental results has indicated that the present model is competent for evaluating the coupled influence of both the constituents and precipitates on the ductility and fracture toughness of heat-treatable aluminum alloys.

4.2. Influence of stress triaxiality level

The constituents are brittle and so are ready to break under external service loading. The breaking percentage should be dependent not only on the constituent characteristics and size but also on the stress conditions. When the specimens are exposed to a higher hydrostatic stress (σ_m), more constituent will crack and both the ductility and the fracture toughness should decrease. The cumu-

lative probability of cracking of particles (P_f) could be given by

$$P_f = 1 - \exp\left[-\frac{f_c}{f_0}\left(\frac{\sigma_c}{\sigma_f}\right)^m\right], \quad (5)$$

where σ_c is the stress on the constituents and σ_f is the fracture strength of the constituents, f_c is the volume fraction of the constituents and f_0 is the reference volume fraction that will crack at probability of 63.2% under external loading equal to σ_f, and m is the Weibull modulus. From the present experimental results, the m and σ_f are determined as 5.8 and 437 MPa for Al–Cu–Mg alloy and 6.5 and 644 MPa for Al–Mg–Si alloy, respectively, by using a least-squares regression analysis [31]. At the moment of fracture of the specimen, the stress on the constituents could be simply regarded as the sum of tensile stress σ_s and the hydrostatic stress in approximation. Based on this approximation and the relationship between the equivalent stress $\bar{\sigma}$ and σ_s at the condition of uniaxial tension, Eq. (5) can be rewritten as

$$P_f = 1 - \exp\left[-\frac{f_c}{f_0}\left(\frac{\sqrt{2}\bar{\sigma}}{(1+v)\sigma_f}\right)^m\left(1+\frac{(1+v)\sigma_m}{\sqrt{2}\bar{\sigma}}\right)^m\right], \quad (6)$$

where v is the Poisson ratio. Eq. (6) describes the dependence of the percentage of cracked constituents on the stress triaxiality level ($\sigma_m/\bar{\sigma}$), from which it could be quantitatively revealed that the increase in the stress triaxiality level will make more constituents crack. At this moment, the interparticle spacing between neighboring cracked constituents, λ_c', will be described as $\lambda_c' = (2\pi k_c r_c^3/f_c P_f)$. By replacing the λ_c in Eqs. (1) and (2) by λ_c', the influence of stress triaxiality level on the ductility and fracture toughness could be evaluated.

The calculated and experimental dependences of strain to fracture and fracture toughness on $\sigma_m/\bar{\sigma}$ are shown in Figs. 8 and 9, respectively. It is revealed that the increase of stress triaxiality level induces a sharp decrease in both ε_f and K_{IC}. For Al–Cu–Mg alloy containing more constituents, such as >4%, the ductility and fracture toughness decrease even with $\sigma_m/\bar{\sigma}$ increasing up to 1.5. On the contrary, for Al–Cu–Mg alloy containing few constituents, such as <4%, the ductility and fracture toughness will remain unchanged after $\sigma_m/\bar{\sigma}$ achieving a certain value, as shown in Figs. 8(a) and 9. This phenomenon can be explained by the breaking of constituents. If there are more constituents in the specimen, many constituents could survive even under a high stress triaxiality level and so the further increase in stress triaxiality level will induce more breaking of constituents and more decrease in both ductility and fracture toughness. On the other hand, if there are few constituents in the specimen, there will be less constituents that could survive after the stress triaxiality level achieving a somewhat large value, after which both the ductility and the fracture toughness will change much less. From this consideration, more constituents will make the ductility and fracture toughness more sensitive to the stress triaxiality level. This is in agreement with the experimental results (dots in Fig. 8 and 9) that the TS-treated

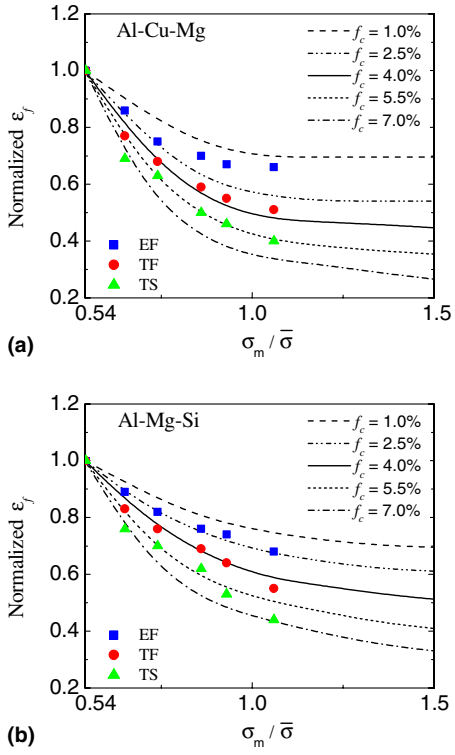

Fig. 8. Dependence of the strain to fracture (ε_f) on the stress triaxiality level ($\sigma_m/\bar{\sigma}$) for (a) Al–Cu–Mg alloy and (b) Al–Mg–Si alloy as a function of the volume fraction of the constituents (f_c). The triangle dots (green), solid dots (red), and square dots (blue) are the experimental results of specimens treated with TS, TF, and EF, respectively. The curves are from the calculations with the present model. (For interpretation of the references in colour in this figure legend, the reader is referred to the web version of this article.)

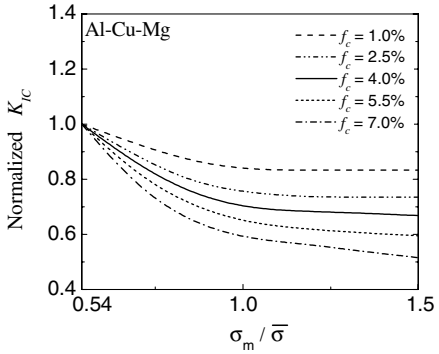

Fig. 9. Calculated dependence of the fracture toughness (K_{IC}) on the stress triaxiality level ($\sigma_m/\bar{\sigma}$) for Al–Cu–Mg alloy as a function of the volume fraction of the constituents (f_c).

specimens exhibit the most sensitive dependence of properties on stress triaxiality level while the EF-treated specimens exhibit the least sensitive dependence.

As presented above, the constituents in Al–Mg–Si alloy (644 MPa) have larger fracture strength than those in Al–Cu–Mg alloy (437 MPa), which means that the constituents in Al–Mg–Si alloy are hard to crack (for example, see Fig. 1). The dependence of ductility and ductile fracture on the stress triaxiality level is then more significant for Al–Mg–Si alloy than for Al–Cu–Mg alloy. Especially for the Al–Mg–Si alloy containing few constituents even of 1%, the decrease of strain to fracture with increasing $\sigma_m/\bar{\sigma}$ is continuous, which is different from the case in Al–Cu–Mg alloy (Fig. 8(a) and (b)).

5. Conclusions

(1) The application of enhanced solution treatment is found to be effective in decreasing the volume fraction of coarse constituents and hence in comprehensively improving the mechanical properties of heat-treatable aluminum alloys.
(2) An unusual non-monotonic dependence of ductility or strain to fracture on the trade-off in volume fraction between the constituents and precipitates is experimentally observed. A multiscale model is presented to explain this dependence reasonably by revealing the coupled influence of both the constituents and precipitates.
(3) The EF-treated specimens have properties that are the least sensitive to the stress triaxiality level while the TS-treated specimens have the most sensitive ones. These experimental results fit well with the calculations based on the multiscale model and a strengthening model.

Acknowledgments

This work was supported by the National Basic Research Program of China (Grant No. 2004CB619303, 2002CB613303). The authors also wish to express their special thanks for the support from the National Natural Science Foundation of China and the National Outstanding Young Investigator Grant of China. Valuable comments and kind suggestions from reviewers are sincerely appreciated too. This work was supported by Program for Changjiang Scholars and Innovative Research Team in University (PCSIRT).

References

[1] Broek D. Eng Fract Mech 1973;5:55.
[2] Cox TB, Low JR. Metall Trans A 1974;5:459.
[3] Hahn GT, Rosenfield AR. Metall Trans A 1975;6:653.
[4] Garrett GG, Knott JF. Metall Trans A 1978;9:1187.
[5] Kaufman JG, Schilling PE, Nelson FG. Met Eng Quart 1969;9:39.
[6] Staley JT. In: Warke WR, Weiss V, Hahn GT (Eds.), Properties related to fracture toughness, ASTM STP 1975;605:71.
[7] Chen KH, Huang LP. Trans Nonferrous Met Soc China 2003;13:484.
[8] Chen KH, Liu HW, Liu YZ. Acta Metall Sinica 2001;37:29.
[9] Staley JT. Aluminum 1979;55:277.
[10] Nan CW, Clarke DR. Acta Mater 1996;44:3801.
[11] Xia Z, Curtin A, Peters WM. Acta Mater 2001;49:273.
[12] Rösler J, Bäker M. Acta Mater 2000;48:3553.
[13] Gokhale AM, Yang S. Metall Mater Trans A 1999;30:2369.
[14] Liu G, Zhang GJ, Ding XD, Sun J, Chen KH. Mater Sci Technol 2003;19:887.
[15] Liu G, Zhang GJ, Ding XD, Sun J, Chen KH. Metall Mater Trans A 2004;35:1725.
[16] DeHoff RT, Rhines FN. Quantitative microscopy. New York (NY): McGraw-Hill; 1968.
[17] Liu G, Zhang GJ, Ding XD, Sun J, Chen KH. Mater Sci Eng A 2003;344:113.
[18] Haynes MJ, Gangloff RP. J Test Eval 1997;25:82.
[19] Mackenzie AC, Hancock JW, Brown DK. Eng Fract Mech 1977;9:167.
[20] Bridgman PW. Studies in large plastic flow and fracture. New York (NY): McGraw-Hill; 1952.
[21] Sun J. Eng Fract Mech 1991;39:P788.
[22] Shercliff HR, Ashby MF. Acta Mater 1990;38:1789.
[23] Deschamps A, Brechet Y. Acta Mater 1999;47:293.
[24] Grong Ø, Shercliff HR. Prog Mater Sci 2002;47:163.
[25] Starink MJ, Wang SC. Acta Mater 2003;51:5131.
[26] Esmaeili S, Lloyd DJ, Poole WJ. Acta Mater 2003;51:3467.
[27] Lloyd DJ. Scrip Mater 2003;48:341.
[28] Shih CF. ASTM STP 1974;560:187.
[29] Dowling NE. Eng Fract Mech 1987;26:333.
[30] Zhu AW, Starke Jr EA. Acta Mater 1999;47:3263.
[31] Liu G. Ph.D. Thesis, Xi'an Jiaotong University, Xi'an, 2002.